

Seismic vulnerability assessment of SMA reinforced concrete bridge pier under near fault ground motions

AHM Muntasir Billah¹, and M Shahria Alam²

¹ The University of British Columbia, Kelowna, Canada

² The University of British Columbia, Kelowna, Canada

ABSTRACT: To explicitly relate the bridge seismic vulnerability with performance objectives, it is necessary to evaluate its seismic fragility considering multi-level performance criteria. To implement such procedures, it is necessary to define damage in terms of engineering performance criteria. In an attempt to improve seismic performance of bridge piers, a hybrid reinforced concrete (RC) bridge pier configuration is considered in this study. The plastic hinge region of the bridge pier is reinforced with superelastic shape memory alloy (SMA) and the remaining portion with regular steel. In this study, various quantitative damage states corresponding to different performance levels (cracking, yielding, strength degradation) is developed for both SMA-RC and steel-RC bridge piers and utilized for analyzing their comparative seismic fragility under the near fault ground motions. The fragility curves provide insight into the failure probability of the bridge piers and aid in expressing the impact of SMA on the bridge pier vulnerability.

1 INTRODUCTION

Bridge infrastructure represents a significant portion of the transportation network of any country. Keeping bridges safe and operational is a major challenge. Bridges are categorized as critical structures as they are highly vulnerable during seismic events (Cruz and Saiidi 2012). Fragility assessment provides an efficient and reliable estimate of the associated risks of highway bridges during a seismic events to a high degree of confidence. Performance-based design aims to adopt a wider range of design scope that results in more predictable seismic performance over the full range of earthquake demand (Hose et al. 2000). To explicitly relate the bridge seismic vulnerability with performance objectives, it is necessary to evaluate its seismic fragility considering multi-level performance criteria. To implement such procedures, it is necessary to define damage in terms of engineering performance criteria. In this study, various quantitative damage states corresponding to different performance levels (cracking, yielding, strength degradation) were developed for both SMA-RC and steel-RC bridge piers and utilized for analyzing their comparative seismic fragility under the near fault ground motions. The strong and long duration velocity pulse associated with the near fault ground motions is known to cause severe ductility demand and residual deformation in bridge piers. The study presented in this paper will assist in evaluating the feasibility of using SMA as reinforcement in bridge piers and its associated seismic vulnerability. This study provides a first step by investigating the influence of SMA as reinforcement in bridge piers under near fault ground motions, as well as its failure probability through the development and comparison of fragility curves.

2 DESCRIPTION OF THE BRIDGE PIERS

2.1 Geometry of bridge piers

This section briefly describes the configuration of SMA-RC and steel-RC bridge pier used in this study. This bridge pier was experimentally studied by Naito et al.(2002) and it was designed following California Bridge Design guidelines (1995). The detailed drawing of the bridge pier is shown in Figure 1, which is a 635 mm square reinforced with 32- M20 steel (diameter 19.5mm), or SMA20 (diameter 20.6mm) longitudinal bars (gross reinforcement ratio of 2.25%). All the piers consisted of deformed M10 ties at 38 mm spacing in plastic hinge length and 70mm outside the plastic hinge length with 19 mm clear cover. The plastic hinge length, L_p was calculated according to Paulay and Priestley (1992) equation:

$$L_p = 0.08 L + 0.022 d_b f_y \quad (1)$$

where, L is the length of the member in mm, d_b represents the bar diameter in mm and f_y is the yield strength of the rebar in MPa.

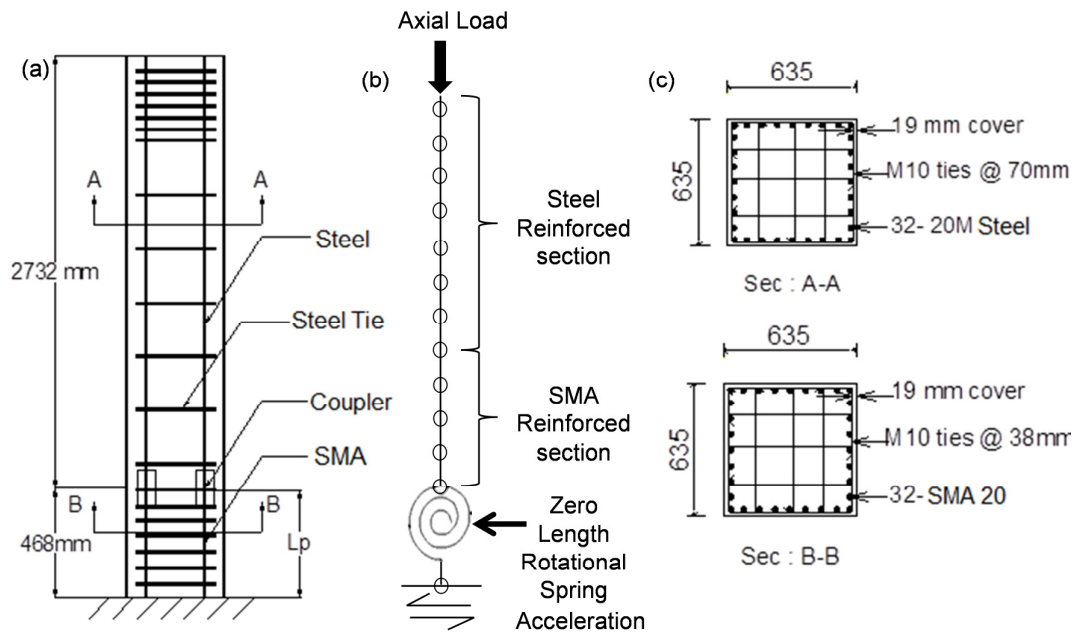


Figure 1: (a) Geometry of the SMA-RC bridge pier, (b) 2D FE model, and (c) Cross section of the pier

The total height (L) of the pier section was 3200 mm and the plastic hinge length (L_p) was calculated as 468 mm according to equation 6. Figure 1 shows the longitudinal distribution of reinforcement for the bridge piers. In the case of SMA-RC bridge pier SE SMA was used as longitudinal reinforcement at the plastic hinge region. SMA bars used here were SMA20 (diameter: 20.6 mm). In the remaining part steel rebars were used as reinforcement. In this paper, unless otherwise stated, SMAs are mainly referred to Ni-Ti SMA (commonly known as Nitinol). Mechanical couplers were used to connect SMA with steel rebars (Alam et al. 2010).

The material properties of concrete, SMA and steel rebar used in the bridge piers are summarized in Table 1.

2.2 Finite element modeling

The analytical model of the bridge pier is approximated as a continuous 2-D finite element using the SeismoStruct nonlinear analysis program (Seismostruct 2011). Nonlinear static pushover and incremental dynamic time-history analyses have been performed on the bridge piers to determine the performances of the SMA-RC and Steel-RC bridge piers. 3-D inelastic beam elements have been used for modeling the piers. Fiber modeling approach has been employed to represent the distribution of material nonlinearity along the length and cross-sectional area of the member.

Table 1 Material properties for SMA-RC and Steel-RC bridge pier

Material	Property	
Concrete	Compressive Strength (MPa)	38.3
	Corresponding strain	0.0029
	Tensile strength (MPa)	3.33
	Elastic modulus (GPa)	29.1
SE SMA	Modulus of Elasticity (GPa)	54.2
	Austenite-to-martensite starting stress (MPa)	414
	Austenite-to-martensite finishing stress (MPa)	530
	Martensite-to-austenite starting stress (MPa)	380
	Martensite-to-austenite finishing stress (MPa)	130
Steel	Superelastic plateau strain length (MPa)	6.2
	Elastic modulus (GPa)	194
	Yield stress (MPa)	485
	Ultimate stress (MPa)	692
	Ultimate strain	0.14
	Plateau strain	0.016

Menegotto-Pinto steel model (1973) with Filippou (1983) isotropic strain hardening property is used for modeling reinforcing steel. Concrete has been modelled using a uniaxial nonlinear constant confinement model, programmed by Madas (1993), that follows the constitutive relationship proposed by Mander et al.(1988) with compressive strength of 38.3MPa and tensile strength 3.33MPa. SMA has been modeled according to the model of Auricchio and Sacco (1997). A constant axial load of 653 kN was applied at the top of the pier to simulate the gravity load.

3 FRAGILITY ASSESSMET METHODOLOGY

3.1 Selection of ground motions

A suite of 20 near fault ground motions are used in this study to develop fragility curves for the SMA-RC and Steel-RC bridge pier. The near fault ground motions are obtained from SAC Joint Venture Steel Project Phase 2 (SAC 2000). The characteristics of the earthquake ground motion records are presented in Table 2. All these ground motions have very high *PGA* ranging from 0.45g to 1.07g with epicentral distances less than 10 km.

Table 2 Characteristics of the earthquake ground motion histories

SL No	Earthquake	Year	Richter Magnitude	Epicentral Distance (km)	PGA (g)	PGV(cm/s)
1	Tabas	1978	7.4	1.2	0.922	108.0
2	Tabas	1978	7.4	1.2	0.958	103.8
3	Loma Prieta	1989	7.0	3.5	0.703	170.0
4	Loma Prieta	1989	7.0	3.5	0.458	89.3
5	Loma Prieta	1989	7.0	6.3	0.672	175.0
6	Duzce, Turkey	1999	7.1	6.3	0.728	56.44
7	Mendocino	1992	7.1	8.5	0.625	123.4
8	Mendocino	1992	7.1	8.5	0.651	91.0
9	Erzincan	1992	6.7	2	0.448	57.0
10	Landers	1992	7.3	2	0.691	133.4
11	Landers	1992	7.3	1.1	0.793	69.0
12	Nothridge	1994	6.7	1.1	0.872	171.0
13	Nothridge	1994	6.7	7.5	0.721	120.0
14	Nothridge	1994	6.7	7.5	0.583	52.9
15	Kobe	1995	6.9	6.4	1.071	157.0
16	Kobe	1995	6.9	6.4	0.563	71.0
17	Kobe	1995	6.9	3.4	0.774	170.5
18	Kobe	1995	6.9	3.4	0.686	156.7
19	Kobe	1995	6.9	4.3	0.673	129.6
20	Kobe	1995	6.9	4.3	0.736	108.4

3.2 Characterization of damage states

Defining a quantitative or qualitative measure for identifying the seismic damage level is an important step in fragility assessment (Erberik et al. 2003). Damage states for bridges or members should be defined in such a way that each damage state indicates a particular level of functionality. In this study four quantitative performance limit states were developed and used to assess the fragility of the SMA-RC and the steel-RC bridge pier. These limit states were developed based on the performance and damage states proposed by Hose et al. (2000). Table 3 shows the four performance limit states and their associated drift limits adopted in this study. The performance limit states considered here are, the drift (%) at the onset of concrete cracking, longitudinal rebar yielding, cover concrete spalling, and crushing of core concrete. The yielding of steel and SMA rebar was assumed to take place at a tensile strain of 0.0025 and 0.00704, respectively. The cracking strain of concrete was considered to be 0.00014 while the spalling strain was assumed to be 0.004 as suggested by Priestley et al. (1996). The cracking strength was calculated according the ASTM C78 formula, ($f_r=0.7\sqrt{f_c'}$), where, f_r is the modulus of rupture and f_c' is the concrete compressive strength in MPa. Dividing f_r by the concrete modulus of elasticity (29.1 GPa), the cracking strain of concrete was calculated to be 0.00014. Paulay and Priestley (1992) found that the crushing strain of confined concrete ranges between 0.015 and 0.05. In this study, the crushing of confined concrete was assumed to take place at a concrete compressive strain of 0.015. In order to determine the limit state drift values for these performance criteria, the drift limits corresponding to the strain values were determined using a regular push-over analysis. The drift limits for the quantitative limit states are provided in Table 3. From the drift limits presented in Table 3, it can be observed that cracking in the SMA-RC bridge pier occurred at a slightly higher drift level compared to the steel-RC bridge pier. This can be attributed to the smoothness of SMA rebar that allowed the SMA to slip more and cause less cracking in the concrete. Similar observations can be made for the spalling drift limits. These findings resemble the experimental results of Saiidi et al. (2009). Interestingly, the

yielding in SMA occurred after the spalling of cover concrete which showed the opposite behavior of the steel-RC bridge pier. A similar observation of the SMA-RC column has been reported by Saiidi and Wang (2006). Before the concrete cracked, both bridge piers exhibited similar stiffness. Once the concrete cracked, the SMA rebars became effective in resisting forces. Since SMA has lower stiffness, there is some reduction in the overall stiffness of the pier. As a result, the SMA-RC bridge pier encountered higher deformation before yielding compared to the steel-RC bridge pier. This lower cracked stiffness of the SMA-RC bridge pier would increase the vibration period of the column, thus reducing the earthquake forces (Saiidi et al. 2009). Before the crushing of confined concrete, the SMA-RC bridge pier sustained higher deformation as compared to the steel-RC bridge pier. This finding is also consistent with the experimental findings of Saiidi et al. (2009).

Table 3 Damage states of bridge piers in terms of performance criteria

Damage State	Performance Level	Functional Level	Description	Drift, Δ (%)	
				Steel-RC	SMA-RC
Slight (DS=1)	Cracking	Fully Operational	Onset of cracking	$\Delta > 0.19$	$\Delta > 0.21$
Moderate (DS=2)	Yielding	Operational	Theoretical first yield of longitudinal rebar	$\Delta > 1.06$	$\Delta > 1.46$
Extensive (DS=3)	Initiation of Local Mechanism	Life safety	Onset of concrete spalling	$\Delta > 1.28$	$\Delta > 1.35$
Collapse (DS=4)	Strength Degradation	Collapse	Crushing of core concrete	$\Delta > 2.98$	$\Delta > 3.14$

3.3 Seismic response analysis

Incremental Dynamic Analyses (*IDA*) were performed using the selected 20 earthquake records for the steel-RC and the SMA-RC bridge pier. In this study, only one horizontal component of the ground motion was considered. The strong horizontal component having a higher *PGA* was selected and used in this study. In order to conduct the dynamic analysis, a point mass (40.5 ton) was assigned to each pier. All the permanent weight at the cap beam level that moves with the pier top was lumped at the pier top. In order to determine the performance limit states, the displacement corresponding to each *DS* was obtained from time history responses. At each level of the *IM*, the bridge pier response were recorded for all 20 earthquake records.

3.4 Development of fragility curves

Fragility curves allow the evaluation of seismic risk of a structure. Fragility functions describe the conditional probability, i.e. the likelihood of a structure being damaged beyond a specific damage level for a given ground motion intensity. In this study probabilistic seismic demand model (*PSDM*) was used to derive the fragility curves which help to express the effect of different reinforcement on the seismic demand placed on the bridge pier. Two approaches are used to develop the *PSDM*: the scaling approach (Zhang and Huo 2009) and the cloud approach (Nielson and DesRoches 2007, Billah et al. 2013). In the current study, only the cloud method was utilized in evaluating the seismic fragility functions of both the columns and buildings. In the cloud approach, a regression analysis is carried out to obtain the mean and standard deviation for each limit state by assuming the power law function (Cornell et al. 2002), which gives a logarithmic correlation between the median *EDP* and the selected *IM*:

$$EDP = a (IM)^b \text{ or, } \ln(EDP) = \ln(a) + b \ln(IM) \quad (2)$$

where, a and b are unknown coefficients which can be estimated from a regression analysis of the response data collected from the nonlinear time history analyses.

An example *PSDM* of the SMA-RC and steel-RC bridge pier, in terms of the performance criteria i.e. cracking, yielding, spalling, and crushing, is shown in Figure 2. From the figure, it is evident that the steel-RC pier yielded an increased dispersion in demand (β_{DIM}) while the SMA-RC pier exhibited a reduced dispersion in demand. On the other hand, the steel-RC increased the median value of the demand placed on the columns, exhibited by an increase in the parameters affecting both the intercept ($\ln(a)$) and the slope (b) of the regression model. The dispersion of the demand, $\beta_{EDP/IM}$, conditioned upon the IM can be estimated from Equation 3 (Baker and Cornell 2006).

$$\beta_{EDP/IM} = \sqrt{\frac{\sum_{i=1}^N (\ln(EDP) - \ln(aIM^b))^2}{N-2}} \quad (3), N = \text{number of total simulation cases}$$

With the probabilistic seismic demand models and the limit states corresponding to various damage states, it is now possible to generate the fragilities (the conditional probability of reaching a certain damage state for a given IM) using Equation 4 (Nielson and DesRoches 2007).

$$P[LS/IM] = \varphi\left[\frac{\ln(IM) - \ln(IM_n)}{\beta_{comp}}\right]; \quad (4)$$

where, $\varphi[]$ is the standard normal cumulative distribution function and

$$\ln(IM_n) = \frac{\ln(S_c) - \ln(a)}{b} \quad (5)$$

$\ln(IM_n)$ is defined as the median value of the intensity measure for the chosen damage state, a and b are the regression coefficients of the *PSDMs*, and the dispersion component is presented in Equation 6 (Nielson and DesRoches 2007).

$$\beta_{comp} = \frac{\sqrt{\beta_{EDP/IM}^2 + \beta_c^2}}{b} \quad (6)$$

where, S_c is the median and β_c is the dispersion value for the damage states of the bridge pier.

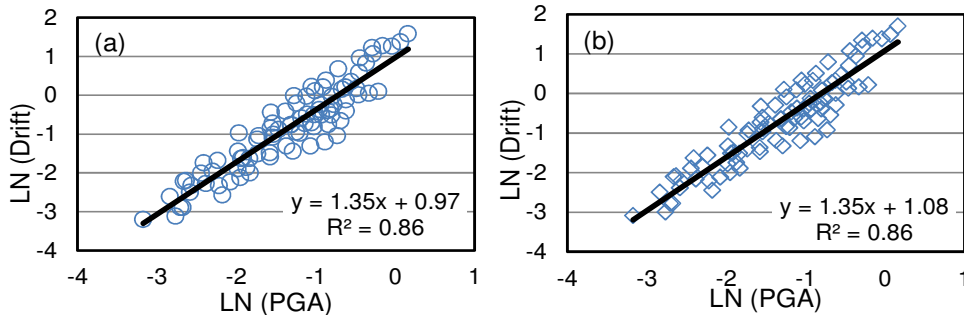


Figure 2: Comparison of the *PSDMs* for (a) SMA-RC, (b) Steel-RC bridge piers

Using the steps described above, the fragility curves for the SMA-RC and steel-RC bridge pier were developed. Figure 3 shows the fragility curves obtained for the SMA-RC and the steel-RC bridge piers for different performance criteria. From Figure 3, it is evident that under a given level of earthquake intensity, the bridge pier with SMA in the plastic hinge region has a lower probability of spalling (DS=3) and crushing (DS=4) as compared to the steel-RC bridge pier. Interestingly, the steel-RC bridge pier has a slightly higher probability of cracking (DS=1) than SMA-RC bridge pier. This is in agreement with previous studies (Saiidi et al. 2009), which found that the cracking of cover concrete becomes more prevalent in the steel-RC bridge pier compared to the SMA-RC pier. On the other hand, the SMA-RC bridge pier is more vulnerable in DS=2 (yielding) which can be attributed to the lower yield strength of SMA as compared to the regular steel.

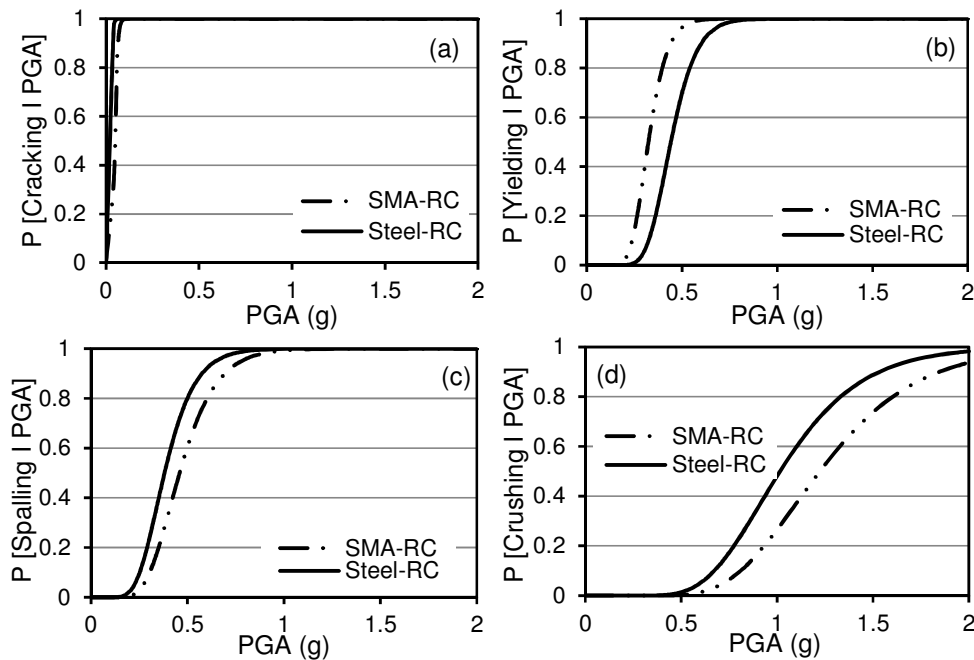


Figure 3: Fragility curves for the SMA-RC and Steel-RC bridge piers for: (a) cracking, (b) yielding, (c) spalling and (d) crushing

4 CONCLUSIONS

This study utilizes analytical simulation method to conduct seismic fragility assessment of RC bridge piers reinforced with steel and SMA reinforcement. Within the scope of this study, a performance based seismic assessment of bridge piers considering performance criteria has been carried out using probabilistic framework. Significant reduction in the vulnerability, in terms of performance criteria, is seen when SMA is used as reinforcement in the plastic hinge region. This can be attributed to the larger drift capacity associated with the SMA-RC bridge pier, although the higher drift capacity does not appear to be a major advantage. The replacement of steel rebars with SMA in the plastic hinge region results in a major difference not only in post-earthquake performance enhancement, but also during the seismic event, by reducing the vulnerability in terms of performance criteria. All these factors rendered the SMA-RC bridge

pier less vulnerable (25% at a PGA of 0.5g) in the higher damage states when compared with the steel-RC bridge pier.

References

- Alam, M.S., Youssef, M.A. and Nehdi, M. 2010. Exploratory investigation on mechanical anchors for connecting SMA bars to steel or FRP bars, *Materials and Structures*, 43: 91-107.
- Auricchio, F. and Sacco, E. 1997. Superelastic shape-memory-alloy beam model, *J Intelligent Materl Syst Struct*; 8(6):489–501.
- Baker, J.W., Cornell, C.A., 2006. Vector-valued ground motion intensity measures for probabilistic seismic demand analysis. *Pacific Earthquake Engineering Research report 2006/08*, PEER Center, University of California Berkeley.
- Billah, A.H.M.M., Alam, M.S. and Bhuiyan, A.R., 2013. Fragility analysis of retrofitted multi-column bridge bent subjected to near fault and far field ground motion. In press, *ASCE Journal of Bridge Engineering*, DOI:10.1061/(ASCE)BE.1943-5592.0000452.
- Caltrans, 1995, Bridge Design Specifications, California Department of Transportation, Division of Structures, Sacramento, Calif.
- Cornell, A.C., Jalayer, F., Hamburger, R.O., 2002. Probabilistic basis for 2000 SAC federal emergency management agency steel moment frame guidelines. *J. Struct. Eng.*, 128, 526–532.
- Cruz, N.C., and Saiidi, M., 2012. Shake-table studies of a four-span bridge model with advanced materials. *J. Struct. Eng.*, 138(2), 183–192.
- Erberik, M.A. and Elnashai, A.S., 2003, Seismic Vulnerability of Flat-Slab Structures, *Mid-America Earthquake Center Report*, DS-9 Project, Civil and Environmental Engineering Department, University of Illinois at Urbana–Champaign; Urbana, IL.
- Filippou, F.C., Popov, E.P., Bertero, V.V. 1983. Modelling of R/C joints under cyclic excitations, *ASCE Journal of Structural Engineering*; 109(11): 2666-2684.
- Hose, Y., Silva, P., Seible, F., 2000. Development of a performance evaluation database for concrete bridge components and systems under simulated seismic loads. *Earthq. Spectra*, 16(2): 413-442.
- Madas P. 1993. *Advanced Modelling of Composite Frames Subjected to Earthquake Loading*, PhD Thesis, Imperial College, University of London, London, UK.
- Mander J.B., Priestley M.J.N., Park R. 1988. Theoretical stress-strain model for confined concrete, *Journal of Structural Engineering*, 114(8):1804-1826.
- Menegotto, M. and Pinto, P.E. 1973. Method of analysis for cyclically loaded R.C. plane frames including changes in geometry and non-elastic behaviour of elements under combined normal force and bending, *Symposium on the Resistance and Ultimate Deformability of Structures Acted on by Well Defined Repeated Loads*, International Association for Bridge and Structural Engineering, Zurich, Switzerland, pp. 15-22.
- Naito, C.J., Moehle, J.P. and Mosalam, K.M. 2002. Evaluation of bridge beam-column joints under simulated seismic loading,” *ACI Structural Journal*, 99(1).
- Nielson, B.G., and DesRoches, R., 2007. Seismic fragility curves for typical highway bridge classes in the Central and South-eastern United States. *Earthquake Spectra*, 23,615–633.
- Paulay, T. and Priestley, M.N.J. 1992. Seismic design of reinforced concrete and masonry buildings, *New York: John Willey & Sons, Inc.*
- Priestley, M.J.N., Seible, F., Calvi, G.M., 1996. Seismic design and retrofit of bridges. *Wiley, New York.*
- Saiidi, M.S., and Wang, H., 2006. Exploratory study of seismic response of concrete columns with shape memory alloys reinforcement. *ACI Struct. J.*; 103(3): 435-42.
- Saiidi, M.S., O’Brien, M., and Zadeh, M.S., 2009. Cyclic response of concrete bridge columns using superelastic nitinol and bendable concrete. *ACI Struct J.*, 106(1): 69-77.
- SeismoSoft. 2011. SeismoStruct - A computer program for static and dynamic nonlinear analysis of framed structures, V 5.0.5 [online], available from URL: www.seismosoft.com.
- SAC Steel Project (2000) 1301 S. 46th Street, Richmond, CA. Available at: http://nisee.berkeley.edu/data/strong_motion/sacsteel/motions/nearfault.html.
- Zhang, J., and Huo, Y., 2009. Evaluating effectiveness and optimum design of isolation devices for highway bridges using the fragility function method. *Engineering Structures*, 31, 1648-1660.